Plasma Chemistry and Plasma Processing (2019) 39:643–666
https://doi.org/10.1007/s11090-019-09981-w

ORIGINAL PAPER

Formation of Nitrogen Oxides by Nanosecond Pulsed Plasma Discharges in Gas–Liquid Reactors

Robert J. Wandell[1] · Huihui Wang[1] · Radha K. M. Bulusu[1] · Rachel O. Gallan[1] · Bruce R. Locke[1]

Received: 20 November 2018 / Accepted: 17 March 2019 / Published online: 29 March 2019

Abstract
A gas–liquid-film flow reactor with a nanosecond pulsed power supply was utilized to produce nitrogen oxides from Ar/N_2 mixtures (gas phase) and deionized water (liquid phase). Chemical analysis of the stable products found in both the gas and liquid phases was performed and chemical quenching was incorporated for the liquid phase samples in order to eliminate post plasma reactions. Significant amounts of NO and NO_2 in the gas phase and NO_2^- and NO_3^- in the liquid phase were determined using FTIR spectroscopy and ion chromatography, respectively. The production rate of all nitrogen oxides produced increased significantly with N_2 concentration while H_2O_2 formation decreased slightly. The gas temperature of the plasma was approximately 525 K and was unaffected by N_2 concentration while the electron density ranged from 1×10^{17} cm^{-3} in pure Ar to 5.5×10^{17} cm^{-3} in 28% N_2. The role of the ·OH in the reaction pathway was assessed by adding CO as a gas phase radical scavenger showing that ·OH is essential for conversion of the gas phase NO and NO_2 into water soluble NO_2^- and NO_3^-. Conversely, atomic oxygen originating from water is likely responsible for NO and NO_2 generation. Experiments with N_2/O_2/Ar mixtures and air showed a significant increase in NO_2 production caused by the additional generation of reactive oxygen species. An overall energy yield for all nitrogen oxides produced in the most efficient case was 50 eV/molecule.

Keywords Non-thermal plasma · Nitrogen fixation · Plasma activated water · Nanosecond discharge · Nitrogen oxides

Introduction

The generation of nitrogen oxides (e.g., NO and NO_2) from N_2 and O_2 in thermal and non-thermal plasma reactors has been extensively investigated over the last approximately 100 years [1–4]. In plasma reactors containing air or mixtures of nitrogen and oxygen, N_2 and O_2 react with plasma generated electrons in a number of different ways

✉ Robert J. Wandell
rjw05c@my.fsu.edu

[1] Department of Chemical and Biomedical Engineering, FAMU-FSU College of Engineering, Florida State University, Tallahassee, FL 32310-6046, USA

including direct dissociation and excitation, and typically the limiting step in the formation of higher oxides of nitrogen is the endothermic formation of nitric oxide, NO [1, 5]. While it has been found that vibrational excitation rather than thermal dissociation of N_2 can lead to a significant increase in the energy efficiency of NO formation, the energy efficiency of NO production with plasma is typically limited by the back reaction of NO with N atoms. Therefore, a quenching step utilizing steep cooling gradients with low pressure non-thermal microwave plasma has led to higher efficiency of NO synthesis from air [1, 6, 7]; however, the cost of such cooling and quenching steps needs further consideration and further oxidation of NO to higher oxides of nitrogen presents additional opportunities for improvements in nitrogen fixation efficiency.

On the other hand, over the last 30 years plasma reactors have also been extensively studied for the removal of nitrogen oxides from combustion and other gases for air pollution control [8–10] through direct and indirect reactions to form liquid soluble products such as nitrite (NO_2^-) and nitrate (NO_3^-) [11–25]. In dry gases, the removal of NO from combustion gas involves the oxidation of NO to NO_2, and in both direct and indirect plasma, ozone, O_3, may play an important role in this step [26–28]. The addition of catalysts and utilization of nanosecond pulses have also been found to enhance NO removal from exhaust gases [29–31]. The addition of water to the plasma leads to the formation of hydroxyl radicals (·OH) through water dissociation (and other reactions [32]) and these radicals lead to the formation of NO_2^-, NO_3^-, and peroxynitrite, $ONOO^-$, causing significant decreases in pH due to the formation of the corresponding acids [33–37]. Water can be added in the form of vapor or as a mist, or the plasma can directly touch the liquid phase leading to water evaporating directly into the plasma [38–40]. Such low energy intensive chemical quenching provides an alternative method to produce higher oxides of nitrogen by rapid conversion of NO and NO_2 into products that are quickly absorbed into the liquid where they are less susceptible to degradation by the plasma and where reverse reactions are minimized.

In gas–liquid (argon-water) plasma high efficiency of hydrogen peroxide (H_2O_2) has been demonstrated in a water spray plasma reactor [41, 42] and in a water film reactor [43], and combinations of H_2O_2 and various nitrogen oxides are formed in air and N_2/O_2 plasma contacting water [44]. Since H_2O_2 and NO_3^- have very high Henry's Law constants, specifically in comparison to NO and NO_2 [45], under atmospheric conditions the former two species are rapidly absorbed into the liquid phase; although some H_2O_2 exists in the gas no HNO_3 is expected in the gas phase due to the rapid absorption.

Mixtures of such reactive oxygen species (ROS) (e.g., H_2O_2 and ·OH) and reactive nitrogen species (RNS) (e.g., NO, NO_2^-, NO_3^-, $ONOO^-$) formed in plasma reactors with water and air (or mixtures with oxygen and nitrogen) have been termed "plasma activated water" (PAW) and have found recent applications and interests in medicine and agriculture [46–49]. For example, in agriculture the generation of nitrogen oxides with non-thermal plasma has been identified as a promising "green" alternative to the conventional Habor Bosch process [50, 51].

The reaction mechanisms and pathways of plasma nitrogen fixation of dry air and N_2/O_2 mixtures [52] and gas–liquid systems [53, 54] including post plasma reactions [55] have been analyzed through kinetic modeling. Both experiments and modeling have shown the importance of the post plasma reactions in PAW as well as the key peroxynitrite pathway in water [37, 56–58]. While the occurrence of the post-plasma peroxynitrite pathway has been proposed as a main reason for the relatively long-lasting antimicrobial properties of PAW, it also significantly complicates chemical analysis of plasma

treated liquid water. This is particularly true for distinguishing reactions that occur in the plasma zone verses those that occur in the post-plasma reactions.

The present study utilizes a continuously flowing gas/liquid plasma reactor where the liquid and gas phases exit the system after plasma treatment upon which immediate chemical quenching can be incorporated to eliminate post-plasma reactions in the liquid effluent, and the gas and liquid products can be quickly and directly determined. The gas phase was analyzed using a FTIR flow cell immediately following the plasma reactor and the chemically quenched liquid samples were analyzed with ion chromatography. This work reports the formation of the stable gas and liquid phase products generated by the non-thermal plasma contacting with liquid water with nitrogen present before post-plasma reactions take place to allow for assessment of the products generated by the plasma discharge alone. Mixtures of N_2/Ar and N_2/Ar/O_2 were utilized in the feed gas to assess the role of reactive oxygen species verses ·OH in the reaction pathway and carbon monoxide (CO) was used as an ·OH scavenger to determine gas phase production of this species [59].

Experimental Methods

A process schematic for the experimental setup used in this study is shown in Fig. 1. Liquid water, delivered at 5 mL/min by a high-pressure reciprocating pump, was mixed with argon (414 kPa, 60 psig) in a mixing zone (1.6 mm Swagelok tee joint) before

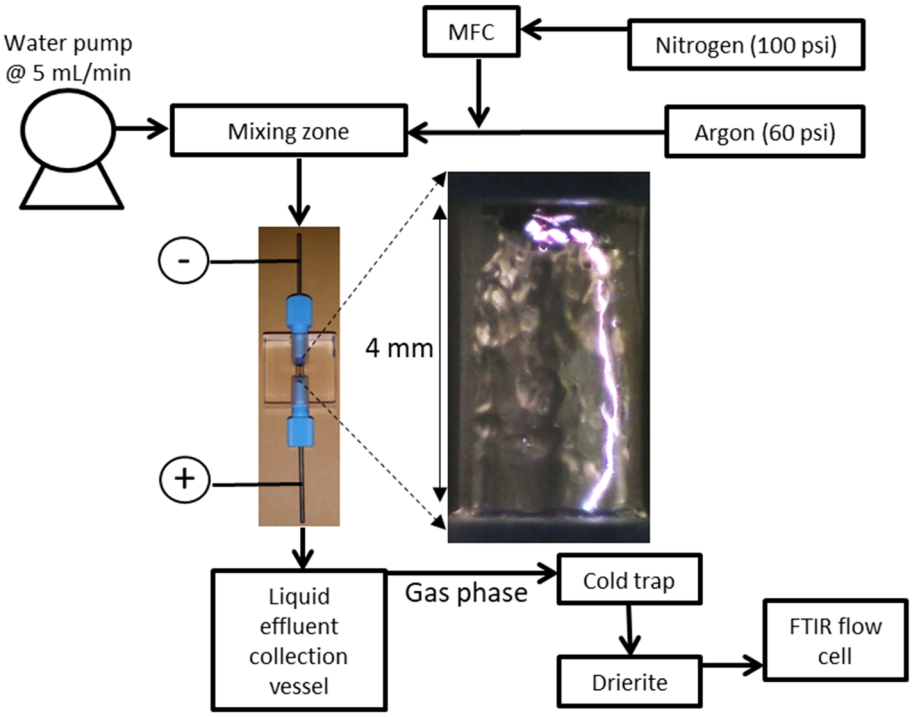

Fig. 1 Process schematic of the experimental setup used in this study. Photo taken at 1/8000 s exposure shows one plasma channel propagating along the gas/liquid interface

entering the inlet of the plasma reactor (0.5 mm ID stainless-steel capillary). The small inner diameter of the inlet capillary limited the total gas flow into the reactor to 3.4 L/min. With this setup the residence times for the liquid and gas were 127 ms and 4 ms, respectively [60]. A mass flow controller (Brooks, 5850E) was used to add N_2 to Ar in order to achieve various N_2/Ar concentrations while maintaining a constant total gas flow rate. A second mass flow controller was employed in experiments where CO or O_2 were added to the N_2 and Ar mixture.

When the gas/liquid mixture enters the discharge region of the reactor a flowing liquid film is formed along the inner walls of the tube and is accompanied by a gas phase flowing though the central core [60]. The stainless-steel inlet and outlet capillaries of the plasma reactor also function as the anode and cathode, respectively. A nanosecond power supply (Eagle Harbor Technologies, Inc.) was connected across the electrodes to produce a filamentary plasma channel which propagates along the interface of the liquid film. The same output settings on the power supply were used for all experiments in this work; 16 kV, 40 ns, 10 kHz. Due to the very short residence times of the gas and liquid phases in the reactor, the reactor quickly reaches steady state after the plasma is turned on. Based on the liquid/gas residence times and the pulse frequency (10 kHz), 1270 pulses occur during the residence time of the liquid (127 ms) while 40 occur for the gas phase (4 ms).

After exiting the plasma reactor, the liquid phase was collected in a sampling vessel while the gas phase flowed directly to an FTIR spectrometer (Jasco – 6700) equipped with a 5 m gas flow cell. Prior to entering the flow cell, the gas phase passed through a dry-ice/acetone cold trap followed by a DIERITE® packed bed to remove remaining water which due to its large dipole moment causes significant interference with the FTIR measurement. For experiments where CO was used, the CO_2 concentration in the gas phase effluent was also quantified using FTIR. More details on the gas phase measurement including sample spectra can be found in the "Appendix".

The NO_2^- and NO_3^- in the liquid phase of the effluent were analyzed using ion chromatography (Dionex, Aquion). Due to the occurrence of post-plasma reactions between H_2O_2 and NO_2^-, the liquid phase of the effluent was discharged into a solution of NaOH to slow down the reaction rate of the peroxynitrite reaction pathway for accurate quantification of the concentrations exiting the reactor [58]. For H_2O_2 measurements, the effluent was discharged into a sodium azide solution to rapidly remove NO_2^- from the solution before quantification with the $TiSO_4$ colorimetric method using a UV–Vis spectrometer (PerkinElmer, Lambda 35) [58, 61]. The conductivity and pH were determined in separate samples without the addition of NaOH or sodium azide. More details on the liquid phase measurement can be found in the "Appendix".

Voltage and current were measured with an oscilloscope (Tekronix MDO 3014; Beaverton, OR, USA) equipped with two high voltage probes (TektronixP6015A, 1/1000; Beaverton, OR, USA) in conjunction with a Rogowski coil (Pearson Electronics, model 6585; Palo Alto, CA, USA). Energy per pulse was determined by integrating the instantaneous power ($V \times I$) across the entire pulse as in Eq. 1.

$$\text{Energy per pulse} = \int (V \times I) dt \tag{1}$$

V Instantaneous voltage
I Instantaneous current
T Time

The energy yield for chemical species produced was determined by dividing the average discharge power by the rate of production. More details on the electrical measurement including temporal probe alignment can be found in the "Appendix" as well as in previous publications using the same system [60, 62].

Time averaged electron density and gas temperature of the plasma were estimated using optical emission spectroscopy (Avantes, AvaSpec-ULS3848; wavelength range: 300–403 nm for gas temperature, 600–700 nm for electron density). For N_2 concentrations less than 5%, gas temperature was determined using ·OH (A–X) from 305 to 320 nm using the same method from our previous work, i.e. two temperature fitting of the Boltzmann plot obtained using Massive OES [62–65]. For higher concentrations of N_2, the gas temperature was determined with the N_2 (C-B) at 337 nm following the fitting protocol in Vorac et al. using Massive OES [64, 65]. Electron density was estimated using Stark broadening of the H_α peak at 656.3 nm using two-Voigt function. More details of this measurement can be found in the "Appendix" as well as our previous work [62, 63, 66, 67].

All measurements were repeated in triplicate and the error bars found throughout this manuscript represent plus and minus one standard deviation from the mean.

Results and Discussion

The focus of this work is chemical species analysis, however, for assessment and comparison of chemical species generation in this plasma system to other plasma and non-plasma processes, measurement of the electrical and plasma properties as well as visual observations of the plasma are essential.

Figure 2 and Table 1 show the electrical properties of the discharge for various concentrations of N_2 in Ar. At 28% N_2 the total energy dissipated per pulse increased by approximately a factor of 2 when compared to pure Ar. The peak current was unaffected by increasing N_2 and the peak voltage (breakdown voltage) increased by 10%. The increase in breakdown voltage is consistent with Paschen's law where the breakdown voltage for N_2 is higher than argon [68]. The slight increase in breakdown voltage provides one cause of the

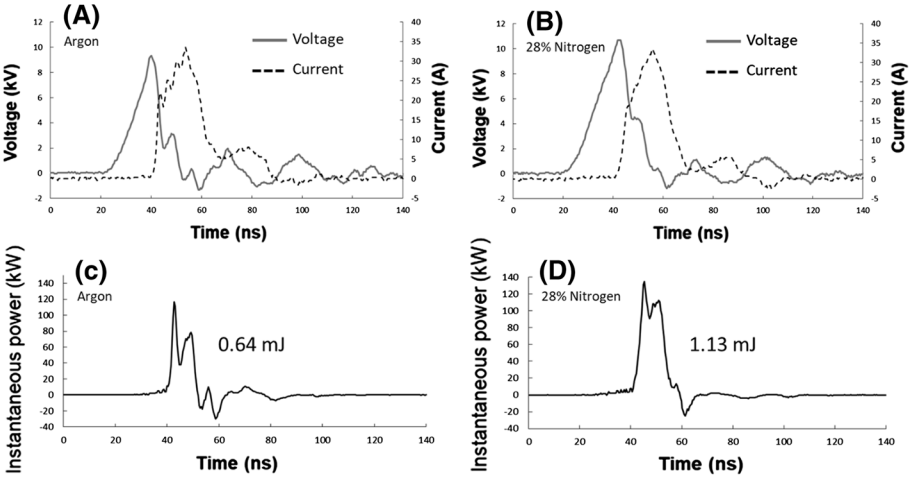

Fig. 2 Voltage and current waveforms (**a**, **b**) and instantaneous power (**c**, **d**) for pure Ar and 28% N_2

Table 1 Electrical measures for various concentrations of nitrogen in argon

Nitrogen (%)	Energy per pulse (mJ)	Peak voltage (kV)	Peak current (A)	Average discharge power (W)
0.00	0.64	9.83	33.47	6.37
0.06	0.76	9.20	32.40	7.59
0.71	0.75	8.87	32.00	7.48
1.77	0.78	9.61	32.67	7.82
3.55	0.82	9.16	31.87	8.21
7.10	0.84	9.40	32.00	8.39
14.19	1.08	9.83	31.33	10.76
21.29	1.08	10.73	33.07	10.76
28.39	1.13	10.81	33.07	11.35

significant increase in total energy. When the instantaneous powers ($I \times V$) for pure Ar and the 28% N_2 mixture are compared (c and d of Fig. 2) it also appears that the pulse duration is slightly longer with N_2 added and this also contributes to the higher energy per pulse. No significant changes of the voltage and current were found with the addition of O_2 or CO at the concentrations utilized, 0–15% and 0–5%, respectively.

The electron density and gas temperature for the plasma discharge are shown in Fig. 3 for various concentrations of N_2 in Ar. The gas temperature was found to be approximately 525 K and was unaffected by the N_2 concentration. A linear increase in electron density was found with increasing N_2 concentration. With no N_2 present the electron density was 1×10^{17} cm^{-3} while at 28% N_2 the electron density increased to 5.5×10^{17} cm^{-3}. OES measurements were not performed for the experiments with the addition of O_2 or CO, however, because no change in discharge power was observed at the relatively low concentrations utilized, little to no change is also expected in the plasma properties.

To further investigate the lack of significant change in the plasma gas temperature with N_2 concentration while the electron density increased by almost one order of magnitude, the diameter of the plasma channel was estimated. The flux of electrons (current) though a radial cross-section of the plasma channel was utilized to estimate the diameter, and the volume of the generated plasma channels based on the measured variables was determined by Eq. 2 [66].

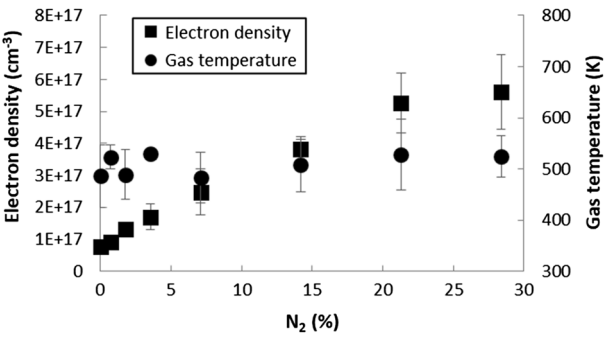

Fig. 3 Gas temperature and electron density as a function of nitrogen concentration

$$V_p = \frac{I_d L^2}{n_e e \mu_e V_d} \tag{2}$$

I_d Discharge current, 33 A (no change)
e Elementary electron charge, 1.602×10^{-19} C (constant)
V_d Discharge voltage, 9.8 kV@0%, 10.1 kV@28%
L Gap distance 0.4 cm, (constant)
n_e Electron density 7.8×10^{16} cm^{-3} @0%, 5.6×10^{17} cm^{-3}@28%
$\mu_e(T_p)$ Electron mobility 245 cm^2/V/s (no change)
V_p Plasma channel volume 0.18 mm^{-3} @0%, 0.22 mm^3 @28%

I_d and V_d were obtained from electrical measurements and n_e from optical emissions. The electron mobility was determined by solving the Boltzmann equation using BOLSIG+ with the plasma temperatures estimated from OES and an estimation of the reduced electric field for parallel plate geometry (V_d/L) [69]. The length of the plasma channel was assumed to be equal to the electrode gap distance (4 mm). The plasma volume in pure argon was estimated using Eq. 2 to be 0.18 mm^3 corresponding to a plasma diameter of 0.24 mm. When 28% N_2 was added to the feed gas, the estimated plasma volume decreased to 0.02 mm^3, corresponding to a diameter of 0.08 mm. The decrease in plasma diameter with increasing N_2 concentration estimated by the current density relation, Eq. 2, was confirmed by measurements taken with high speed imaging shown in Figure 10. Further, the measured values of the plasma diameter found with imaging match well with the current density estimates. From these estimates of plasma volume and electron density, the total number of free electrons can be calculated as a function of nitrogen concentration. Due to the increase in electron density corresponding with a decrease in plasma volume, the total number of electrons remains relatively unchanged when comparing the pure argon case (1.4×10^{13} total electrons) to 28% N_2 (1.3×10^{13}).

Based on the above assessment of the electrical and plasma properties as well as the photograph shown in Fig. 4, the plasma is best described as a filamentary non-thermal plasma channel generated in the gas phase which propagates along the liquid interface [60]. This system is similar to that of a transient spark discharge [70–73]. The plasma generated transient spark discharges are also short-lived filamentary plasma channels (streamers) with an electron density on the same order of magnitude as that found in this study. The energy dissipated per pulse is also similar ($\approx$ 1 mJ). The transient spark discharge with dry air reports significant NO and NO_2 generation and when a water spray was introduced to the transient spark nitrates and nitrites were also produced. A comparison for NO_x generation with transient spark discharges to this work is provided in Table 2.

Potential Chemical Reactions

NO formation in thermal plasmas as well as in combustion processes has been well studied where the generally accepted reaction pathway is the Zeldovich mechanism. In this reaction pathway NO is formed through thermal dissociation of O_2 and N_2 where the high bond strength of N_2 causes the N_2 dissociation to be the rate limiting step [1]. NO production from dry air and non-thermal plasma, where the gas temperature is not high enough for thermal dissociation to dominate (< 5500 K), is initiated through electron impact dissociation and excitation of O_2 (R2) and N_2 (R1) which generate atomic oxygen and various excited states of N_2. The vibrational excitation of N_2 lowers the bond strength of

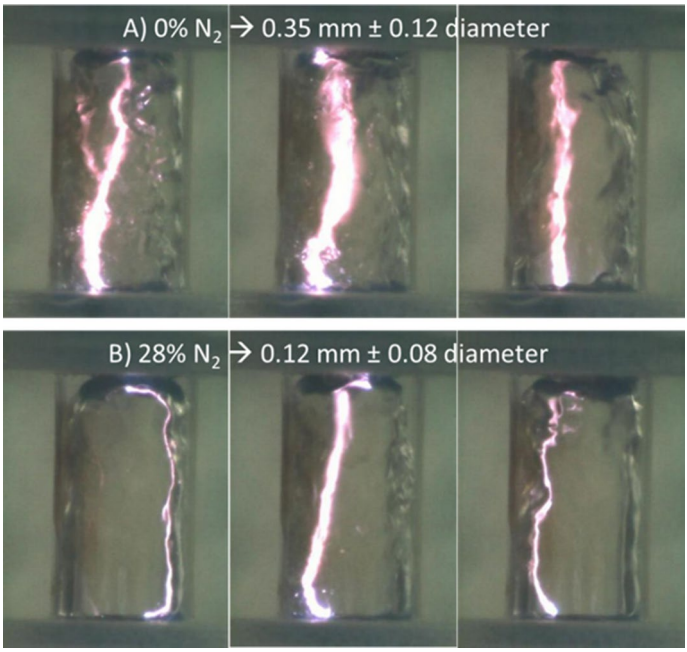

Fig. 4 Various images of a single discharge channel propagating along the gas–liquid interface. Images were taken with a 1/8000 s shutter speed. Plasma diameter was estimated by the software integrated measurement tool (Keyence, VW-9000). The diameters reported represent the average and standard deviation of the images shown. **a** Argon carrier gas, diameter—0.35 mm ± 0.12 **b** 28% N_2 in argon, diameter—0.12 ± 0.08

the molecule and allows for NO generation in non-thermal conditions through reactions with atomic oxygen (R3). Additional NO generation can then also be achieved through Reaction 4.

$$N_2 + e^- \rightarrow N_2^* + e^- \quad \text{(R1)}$$

$$O_2 + e^- \rightarrow O + O + e^- \quad \text{(R2)}$$

$$O + N_2^* \rightarrow NO + N^* \quad \text{(R3)}$$

$$N^* + O_2 \rightarrow NO + O \quad \text{(R4)}$$

This pathway is known as the Zeldovich mechanism stimulated by vibrational excitation [1]. Further oxidation of NO into NO_2 can then be achieved by additional reactions with atomic oxygen and ozone (R5 and R5).

$$NO + O \rightarrow NO_2 \quad 3E-11 \ \frac{cm^3}{mol\,s} \quad \text{(R5)}$$

$$NO + O_3 \rightarrow O_2 + NO_2 \quad 1.8E-14 \ \frac{cm^3}{mol\,s} \quad \text{(R6)}$$

Table 2 Energy yield comparison for other plasma systems

Process	Product	Feed	Conditions	Energy yield (Moles/J)	Energy yield (eV/molecule)	Reference
Birkeland and Eyde	NO	N_2, O_2	Thermal plasma arc	4.1E−07	2.5E+01	Cited in [1]
Birkeland and Eyde	NO	N_2, O_2	Thermal plasma arc	5.6E−07	1.9E+01	Cited in [79]
Birkeland and Eyde	NO	N_2, O_2	Thermal plasma arc	8.7E−07	1.2E+01	Cited in [80]
Thermal plasma	NO	N_2, O_2	20–30 atm, 3000–3500 K	1.2E−06	9.0E+00	Cited in 1 [1]
Microwave non thermal plasma	NO	N_2, O_2	Magnetic field and cooled walls	3.5E−06	3.0E+00	Cited in 1 [1]
Low pressure	NO	N_2, O_2	With catalyst	1.2E−06	8.7E+00	Mutel, cited in [81]
Plasma jet	NO	N_2, O_2	Varied O_2/N_2 ratio	4.6E−07	2.3E+01	Krop/Pollo, cited in [81]
Plasma jet	NO	Air	3.5 W plasma jet	9.5E−10	1.1E+04	[82]
Rotating disk with injected water	NO	Air		3.1E−07	3.3E+01	Krop/Pollo, cited in [81]
Plasma beam	NO	Air	30 kW	1.0E−06	1.0E+01	Alekesev, cited in [81]
Jet arc	NO			2.8E−07	3.7E+01	Coudert, cited in [81]
Plasmatron gliding arc	NO_3^-	Air with water	240 W	3.4E−09	3.1E+03	[83]
Glow discharge	NO_3^-		420 W 162 MHz	1.8E−09	5.7E+03	[79]
AC gliding arc over water	NO_3^-	Air with water	2 electrodes 300 W	2.9E−08	3.6E+02	[44]
AC gliding arc over water	NO_3^-	Air with water	3 electrodes 600 W	2.4E−08	4.3E+02	[44]
AC gliding arc with spray	NO_3^-	Air with water	3 electrodes 600 W with spray	5.3E−09	2.0E+03	[44]
Bubbling in water	HNO_3	Air with water	Underwater pulsed discharge with bubbles	5.4E−09	1.9E+03	[44]
Transient spark	NO_x	Dry air	Transient spark, DC self-pulsing	1.2E−7	9.0E+1	[70]
Transient spark	NO_x, NO_2^-, NO_3^-	Air with water	Transient spark with electrospray	1.1E−7	9.6E+1	[73]

Once formed, the gas phase NO and NO_2 can be converted into NO_2^- and NO_3^- with the addition of liquid water (R7 and R8). However, solubility of these gasses in water as well as mass transfer resistance limits rapid conversion in this manner.

$$NO_{2(aq)} + NO_{2(aq)} + H_2O \rightarrow NO_2^- + NO_3^- + 2H^+ \quad \text{(R7)}$$

$$NO_{(aq)} + NO_{2(aq)} + H_2O \rightarrow 2NO_2^- + 2H^+ \quad \text{(R8)}$$

When water vapor is present in a non-thermal plasma system, ·OH is formed in abundance through election impact with water molecules in the plasma channel (R9). In cases with high ·OH concentrations, typically with liquid water contacting the plasma, ·OH can combine to form hydrogen peroxide (H_2O_2) (R10) which can then be sequestered in the liquid as a stable product [74]. Alternatively, the ·OH can react to form water and atomic oxygen (R11) which could provide an additional source of the atomic oxygen needed for NO production.

$$H_2O + e^- \rightarrow \cdot H + \cdot OH + e^- \quad \text{(R9)}$$

$$\cdot OH + \cdot OH \rightarrow H_2O_2 \quad 2.6E-11 \ \frac{cm^3}{mol\,s} \quad \text{(R10)}$$

$$\cdot OH + \cdot OH \rightarrow H_2O + O \quad 1.5E-12 \ \frac{cm^3}{mol\,s} \quad \text{(R11)}$$

An alternate pathway for NO generation when water is present is by the reaction of ·OH with atomic nitrogen (R12). Direct conversion of NO into HNO_2 can also be achieved through reaction with ·OH as well as conversion of NO_2 into HNO_3 (R13 and R14). Due to their high rate constants, Reactions 13 and 14 likely play key roles in the generation of water-soluble nitrogen oxides when water is present in non-thermal plasmas. This is analogous to hydrogen peroxide generation where once the product is sequestered into the liquid it is less likely to be degraded by the plasma.

$$N + \cdot OH \rightarrow NO + H \quad 5E-11 \ \frac{cm^3}{mol\,s} \quad \text{(R12)}$$

$$NO + \cdot OH \rightarrow HNO_2 \quad 3E-11 \ \frac{cm^3}{mol\,s} \quad \text{(R13)}$$

$$NO_2 + \cdot OH \rightarrow HNO_3 \quad 3E-11 \ \frac{cm^3}{mol\,s} \quad \text{(R14)}$$

Gas Phase Analysis

Figure 5 shows the concentrations of NO and NO_2 in the gas effluent of the reactor for various N_2/Ar concentrations. Both NO and NO_2 production increase sharply with nitrogen concentration up to 5%. At higher concentrations, NO_2 production levels off while NO production shows a gradual increase. Significantly less NO_2 is produced compared to NO at all N_2/Ar concentrations investigated. This could be explained by NO_2 being a secondary reaction product, NO must first be formed through Reaction 3 followed by an additional reaction with atomic oxygen (R5) to form NO_2. Another consideration is that the

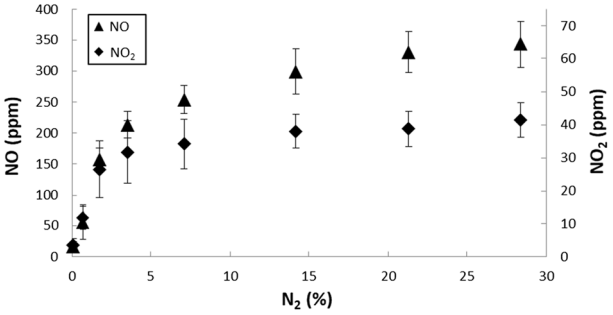

Fig. 5 Gas phase analysis for various N_2/Ar concentrations

reaction rate of O with N_2^* to form NO (R3) is faster than that of O with NO to form NO_2 (R5). The leveling off of NO_2 implies that there is an atomic oxygen limitation at higher N_2 concentrations. The leveling off of NO also suggests a limitation on the availability of atomic oxygen, although another possibility is a limitation in ·OH since NO can be directly formed from ·OH and N (R12). Because no O_2 was present in the feed for these experiments a likely source of atomic oxygen is from water via Reaction 11, this is supported by modeling work with underwater discharges [75, 76]. Reactions 15 and 16 are also potential pathways for O production from water by direct electron collisions and electronically excited water, H_2O^*, respectively.

$$H_2O + e^- \rightarrow 2H\cdot + O + e^- \quad \text{(R15)}$$

$$H_2O^* + H_2O \rightarrow H_2 + O + H_2O \quad \text{(R16)}$$

While no chemical probes for atomic oxygen were employed in this study, confirmation of the presence of this short-lived species was found with optical emission spectroscopy (777 nm). A sample spectrum showing the presence of this band is given in the "Appendix" (Fig. 17). Further experimental and modeling studies are needed to assess the most predominant pathway(s) for O production in this system.

Liquid Phase Analysis

Figure 6 shows the liquid phase products for the various N_2/Ar mixtures. For pure Ar the only stable product found in the liquid phase was H_2O_2 [74]. When only a small amount of N_2 was added (550 ppm) NO_2^- and NO_3^- were detected in the liquid. As the N_2

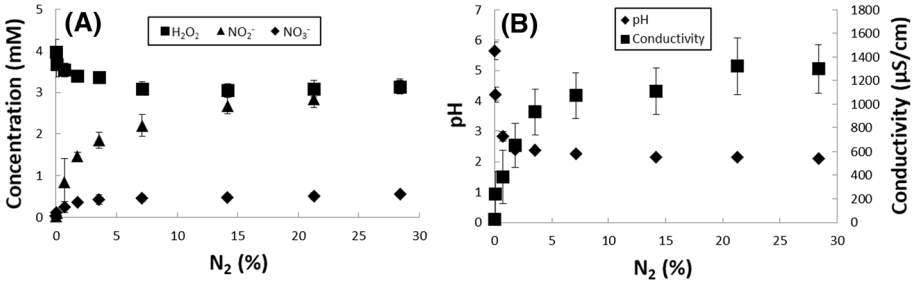

Fig. 6 Liquid phase analysis for various N_2/Ar concentrations. **a** Concentrations of stable chemical species produced **b** pH and conductivity of effluent

concentration increased, the NO_2^- and NO_3^- in the liquid phase increased following the same trends as NO and NO_2 in the gas phase, respectively. This implies that the NO_2^- and NO_3^- measured at the exit of the reactor are formed directly from the reactions of ·OH with gas phase NO and NO_2 (R13 and R14). The decrease in H_2O_2 with increasing N_2 also supports this hypothesis due to ·OH radical scavenging by NO and NO_2 in the gas phase. Here, the drop in H_2O_2 cannot be attributed to post plasma reactions with NO_2^- because the NO_2^- was removed with sodium azide immediately after exiting the reactor. Additional support can also be seen in the significant drop of pH in the liquid effluent as the NO_2^- and NO_3^- concentrations increase. For these reasons the NO_2^- and NO_3^- detected in the liquid are assumed to be in the form of HNO_2 and HNO_3. The simultaneous increase of conductivity and decrease in pH can be correlated to increases of HNO_3 and HNO_2 as shown in Fig. 7.

It should again be noted that if the liquid phase was not quenched at the exit of the reactor, more NO_3^- would be formed in post plasma reactions between NO_2^- and H_2O_2 through the peroxynitrite pathway where after a sufficient period of time all NO_2^- would be converted into NO_3^-. Because the peroxynitrite pathway occurs on the time scale of minutes to hours depending on the concentration and pH of the plasma activated water, and the average liquid residence time in the reactor is only 127 ms, this pathway can be considered to have a negligible effect on the reactions occurring in the plasma reactor assessed in the present study [58].

Figure 8 shows the rates of production of all the major chemical species produced in the N_2/Ar mixtures. Most nitrogen products detected exist in the gas phase and account for over 80% of all nitrogen oxide species, the majority of which are in the form of NO. High concentrations of H_2O_2 are also produced despite the likelihood that a limitation in ·OH is responsible for the lack of conversation of NO and NO_2 into HNO_2 and HNO_3, respectively. This result is consistent with previous analysis of this reactor system that utilized gas and liquid phase radical scavengers to show that H_2O_2 was generated from ·OH near the gas–liquid interface and that H_2O_2 was not strongly affected by ·OH scavenging in the gas phase [78].

The energy yield for total nitrogen oxides produced is shown in Fig. 9 as a function of N_2 concentration. From Fig. 9 the energy cost per molecule decreases as the N_2 concentration increased up to 10% after which it levels off at approximately 50 eV/molecule. Table 2 provides a comparison of the energy yield of this study to other plasma processes.

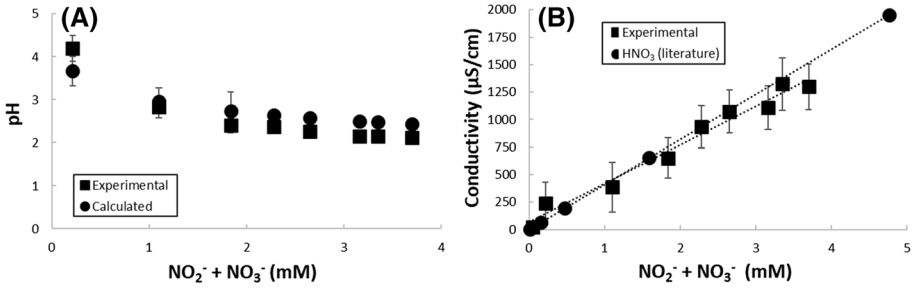

Fig. 7 **a** Comparison of the measured pH of the PAW effluent as a function of nitrite and nitrate concentrations against the calculated pH if it is assumed all NO_2^- and NO_3^- are in the form of HNO_2 and HNO_3. **b** Comparison of the measured conductivity of the PAW effluent as a function of nitrite plus nitrate concentrations against literature values for the conductivity of various HNO_3 solutions [77]

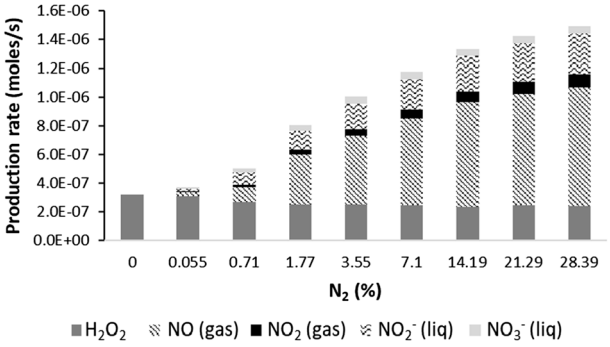

Fig. 8 Production rates of all measured species in the liquid and gas phases as a function of N_2 percentage in feed gas

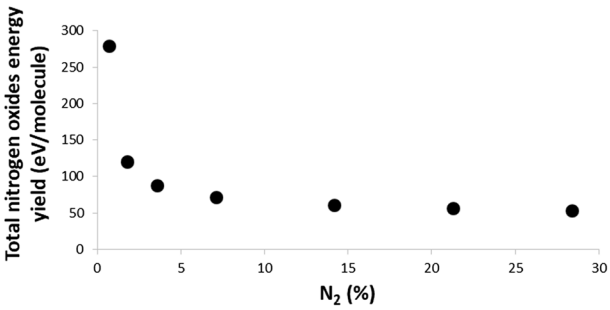

Fig. 9 Energy yield for total nitrogen oxides produced in both the liquid and gas phases as a function N_2/Ar concentration

The formation of nitric oxide, NO, is a long studied reaction in plasma chemistry due to its importance in fertilizer formation. For example, in 1900 Birkeland and Eyde developed a thermal plasma arc furnace which was used commercially to make NO from N_2 and O_2. The thermodynamic limit for this reaction is 1 eV/molecule and the efficiency reported by Birkeland and Eyde was 25 eV/molecule [1]. The highest efficiency for nitrogen fixation with a plasma process was a non-thermal microwave plasma with magnetic field and low pressure (3 eV/mol) however, the cost of attaining the low pressure and the magnetic field were not included [1]. Of the various plasma process listed in Table 2 the transient spark [70–72] has the most closely related plasma properties to this work and the energy yield for total NO_x (NO/NO_2) from air is similar in magnitude to that reported in this study. When an electrospray was combined with the transient spark, nitrate and nitrite were observed in the exiting liquid, however the energy yield for total nitrogen oxides remained similar [73]. It is important to note that the plasma reactor utilized in this work only requires air and water feed and operates at near atmospheric conditions.

·OH Scavenger

To further investigate the role of ·OH in the process, CO was added to the gas phase (0–5%) of the 28% N_2/Ar mixture. CO is an excellent gas phase ·OH scavenger and due to the fast rate of reaction between ·OH and CO (R15), CO added to the gas phase will rapidly react with ·OH radicals and prevent them from participating in reactions with other compounds [78, 84]. The effectiveness of CO as a gas phase ·OH scavenger is illustrated in Fig. 10

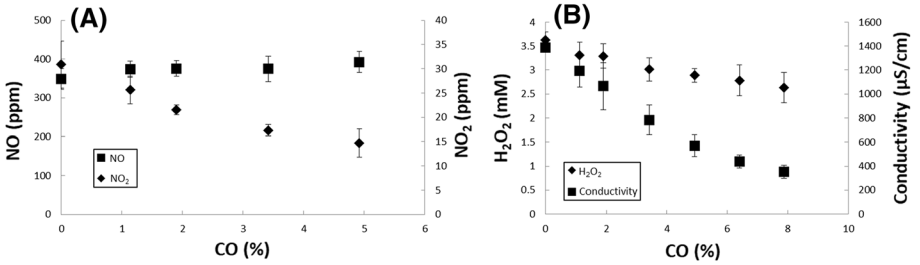

Fig. 10 Chemical analysis of the gas phase (**a**) and liquid phase (**b**) for various concentrations of carbon monoxide added to a 28% N_2/Ar mixture. Conductivity was used as an indicator of changes in NO_2^- and NO_3^- in the liquid phase

where the ·OH consumed in CO_2 production by Reaction 17 increases with CO% added to the gas feed.

$$CO + \cdot OH \rightarrow CO_2 + H \quad 1.87E-13 \ \frac{cm^3}{mol\,s} \tag{R17}$$

For the data shown in Fig. 10, conductivity was used as an indicator of changes in NO_2^- and NO_3^- in the liquid phase. The addition of CO decreased the production of NO_2, NO_2^-, NO_3^-, and H_2O_2 significantly but had little effect on NO. This result clearly indicates that direct ·OH reactions play important roles in NO_2, NO_2^-, and NO_3^- generation, and may not directly react with N via Reaction 12 to a significant degree. With no O_2 present in the feed gas, a reduction in the ·OH concentration will also cause a reduction in the atomic oxygen formed by Reaction 11. Because there are no possible reactions of ·OH to form NO_2, the reduction in NO_2 formation is likely caused by the reduction in availability of atomic oxygen. However, a chemical probe specific to atomic oxygen would be useful to confirm this finding. Since reactions with atomic oxygen are also probable pathways for NO generation, the lack of any significant change in NO concentration is possibly due to a decrease in NO production (R3) being balanced by a decrease in consumption (conversion to NO_2) (R5).

The lower limit on the production of ·OH when no N_2 was present in the feed can be estimated based on the conversion of CO to CO_2 (R17) and H_2O_2 formation (R10). Based on these reactions, for every mole of CO_2 produced one mole of ·OH is consumed while for every mole of H_2O_2 produced two moles of ·OH are consumed. Additionally, the ·OH consumed in the generation of nitrogen oxides was estimated by assuming that all NO and NO_2 are produced by reactions with atomic oxygen (R3 and R5) and that the atomic oxygen is produced by Reaction 11. Thus, for every mole of NO produced two moles of ·OH are consumed, and for NO_2 four moles of ·OH are consumed. If the NO_2^- are NO_3^- are assumed to be produced from reaction of ·OH with NO and NO_2 (R13 and R14), production of NO_2^- equates to three ·OH consumed while NO_3^- equates to five ·OH. This information is summarized in the Table 3.

The production rates of ·OH based on the assumptions in Table 3 are shown in Fig. 11. Figure 11a shows the ·OH production rate when only argon was used as the carrier gas with various concentrations of CO added. As the concentration of CO was increased the measured ·OH production rate increased significantly while the production rate of H_2O_2 slightly decreased as a result of the ·OH scavenging by CO. At 3.4% CO the ·OH production rate was 4×10^{-6} mol/s. These results are similar to experiments performed in the same reactor but utilizing a different power supply based upon

Table 3 Assumed hydroxyl radical consumption based on production of measured products

Reaction	·OH utilized per mole produced
R10	H_2O_2=2OH
R17	CO_2=1OH
R11	O=2OH
R3	NO=2OH
R5	NO_2=4OH
R13	HNO_2=3OH
R14	HNO_3=5OH

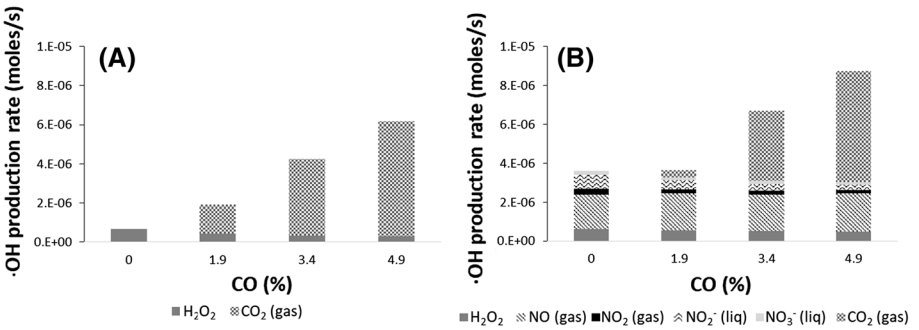

Fig. 11 Estimated hydroxyl radical production rate based on the generation of H_2O_2, CO_2, and nitrogen oxides for various gas mixtures. **a** Ar/CO, **b** 28% N_2/Ar/CO

microsecond pulses where an ·OH production rate of $5x10^{-7}$ mol/s was found at 2.6% CO [78]. Based on the high production rate of ·OH from CO_2 measurements it is clear that significantly more ·OH is produced in the system than can be accounted for by H_2O_2.

Figure 11b shows the ·OH production rate for the 28% N_2/Ar mixture with various concentrations of CO. The ·OH production rate was lower in the case with 1.9% CO in Ar than in the case with 0% CO with 28% N_2 due to the contribution of ·OH scavenged by nitrogen oxides. As the CO concentration was increased, ·OH production continued to increase up to a value of 8.3×10^{-6} mol/s. This result shows that even with the ·OH accounted for in the production of nitrogen oxides and H_2O_2 there is still a significant amount of ·OH that remains unutilized (available to react with CO). The energy yield for ·OH production can also be calculated by dividing the production rate by the corresponding average discharge power. The highest energy yield was found to be 7×10^{-7} mol/J for the case of 28% N_2 and 4.9% CO in balance Ar and this value is in close agreement with the value of 5×10^{-7} mol/J found in the previous work with microsecond pulses and 2.6% CO in Ar in same reactor [78]. This result suggests that the energy yield in a nanosecond discharge is not significantly different than that of a microsecond discharge; however, it can noted that there are other advantages of the nanosecond power supply, including tolerance of high solution conductivity [63].

Oxygen Addition

To further investigate the role of reactive oxygen species in the process, various concentrations of O_2 (0–15%) were added to the 28% N_2/Ar mixture. An additional experiment was performed with air. Results for the gas and liquid phase analyses are shown in Fig. 12. The only significant change measured with the addition of O_2 was a large increase in NO_2 generation. Because NO is a precursor for NO_2, it is likely that NO production also increased but it was rapidly converted to NO_2 due to an increased concentration of reactive oxygen species. This would explain the lack of any net change in NO as O_2 concentration was increased. The lack of an increase in conductivity implies that the NO_2^- and NO_3^- concentrations did not change with added O_2 and provides further evidence that the conversion of NO and NO_2 into these products is limited by ·OH (R13 and R14) and not by other reactive oxygen species.

When air was utilized the results were similar to those with the 15% O_2, 28% N_2, balance Ar mixture. Higher concentrations of NO and NO_2 were observed in the gas phase compared to the case with no O_2; however, little increase was seen in the production of NO_2^- and NO_3^-. This result is again consistent with higher atomic oxygen concentrations leading to an increase in NO and NO_2 generation and with a limitation of ·OH for further conversion of these products to HNO_2 and HNO_3. It should also be noted that no O_3 was detected in the gas phase with FTIR for both the O_2 addition and air experiments. This is consistent with other studies with similar plasma conditions where the lack of ozone was attributed to plasma (gas) temperatures above ambient leading to rapid thermal degradation of O_3 [71, 85, 86]. Additionally, any O_3 which could be formed would rapidly react with NO (R6) [26, 27].

Conclusions

Chemical analysis of the products generated when filamentary non-thermal plasma channels propagate along a flowing liquid water film in N_2/Ar atmosphere shows significant amounts of NO and NO_2 in the gas phase and NO_2^-, NO_3^-, and H_2O_2 in the liquid. By inducing chemical quenching of the liquid effluent, this work decouples the chemical reactions induced by the plasma from those which occur in the post-plasma solution. This allows for assessment of the reaction pathways leading to the generation of these chemical species without the complications induced by secondary interactions of the

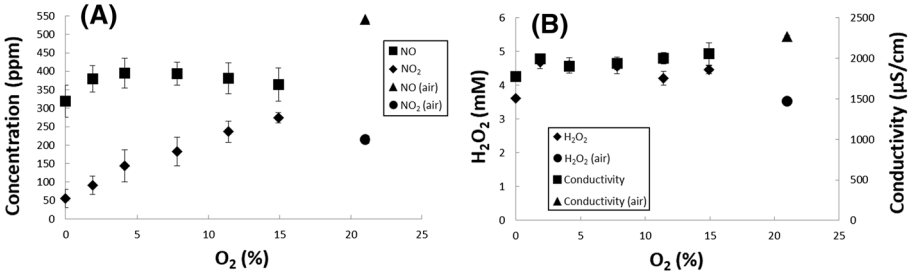

Fig. 12 Chemical analysis of the gas phase (**a**) and liquid phase (**b**) for various concentrations of oxygen added to a 28% nitrogen mixture with balance argon. Experimental results for air are also displayed

plasma generated molecules. Current work is in progress to develop chemical reaction modeling for further assessment of the reaction pathways described in this paper.

In this work the gas temperature of the plasma channel was found to be approximately 525 K and was unaffected by the N_2 concentration. The electron density was 7.8×10^{16} cm^{-3} with no N_2 present (pure Ar) and increased to 5.6×10^{17} cm^{-3} at 28% N_2 in Ar. In contrast, the volume (diameter) of the plasma channel decreased with increasing N_2 resulting in a negligible change in total free electrons with N_2 concentration. The production of all nitrogen oxides increased as a function of the amount of N_2 in the feed gas giving a maximum production rate of 1.5×10^{-6} mol/s at an energy yield of 50 eV/molecule at the highest N_2 concentration investigated (28%). The negligible change in total free electrons with N_2 implies that the significant increase in total nitrogen oxides produced with N_2 was mainly caused by an increased availability of nitrogen and not by an increase of free electrons available for reaction.

This work shows that significant generation of nitrogen oxides is possible without a source of oxygen in the feed gas. The reaction of ·OH to form water and O (R11) is one likely source of the atomic oxygen needed for NO and NO_2 generation, however, other reactions are possible (R15 and R16). NO formation can then proceed though Reaction 3. However, the addition of oxygen to the gas feed did enhance the overall NO_x production by adding an additional atomic oxygen source (R2). ·OH does not otherwise appear to directly affect the generation of NO (R12) or NO_2 but does play a key role in the conversion of NO and NO_2 into HNO_2 and HNO_3, respectively. While further conversion of the remaining gas phase NO and NO_2 into HNO_2 and HNO_3 appears to be limited by ·OH, there is still a significant quantity of ·OH unutilized as evident from CO scavenging (CO_2 production) and H_2O_2 production. Future work should be done to investigate capitalizing on this unutilized ·OH.

Acknowledgements This work was supported by the National Science Foundation (CBET 1702166) and Florida State University.

Appendix

Electrical Measurements

Temporal alignment of current and voltage probes is essential for accurate analysis of nanosecond discharges. For temporal alignment of these probes the nanopulser was discharged across a resistor placed inside the Rogowski coil while the two voltage probes measured the electrical potential across the resistor. The deskew of each voltage probe was then adjusted to ensure simultaneous rise in each voltage probe with current.

For analysis of the plasma discharge, the high voltage probes were connected across the stainless-steel inlet and outlet capillaries to measure the electric potential across the plasma discharge region. The reactor was placed inside the Rogowski coil so that the discharge region was centered within the coil to measure current flow through the discharge region only. With placement of the voltage and current probes in this fashion, the measured values give the electrical potential between the electrodes and current flow only within the formed plasma channels. More details of the electrical analysis can be found in our previous work [60, 62].

H_2O_2 Quantification

For H_2O_2 quantification the effluent was discharged directly into a sodium azide solution of sufficient quantity to rapidly remove all NO_2^- from the liquid phase. 2 mL of effluent from reactor was discharged into a 1 M sodium azide solution at an equal 1–1 volume ratio (i.e. 2 mL sodium azide+2 mL effluent). The H_2O_2 in the resulting solution was then quantified with the $TiSO_4$ colorimetric method using a UV–Vis spectrometer detailed in our previous publications as well as others (PerkinElmer, Lambda 35) [58, 61, 87]. The resulting concentration was then multiplied by a factor of 2 in order to account for the dilution with the sodium azide solution.

Nitrate and Nitrite Quantification

For nitrate and nitrite quantification the pH of the effluent must be rapidly increased to slow/stop the reaction of NO_2^- with H_2O_2. In addition, the solutions were diluted to approximately 10 ppm total nitrogen for protection of the IC instrument. For this procedure, 3 mL of effluent was directly discharged into a 26.7 mL solution of 1 mM NaOH. The pH of the resulting mixture after effluent addition was approximately 10. Calibration curves for the IC were prepared using various dilutions of $NaNO_2$ and KNO_3. All samples were analyzed on a Dionex, Aquion ion chromatograph equipped with an IonPac™ AS22 column (4×250 mm), an AERS™ 500 carbonate suppressor, and a conductivity detector. The eluent was 4.5 mM sodium carbonate mixed with 1.4 mM sodium bicarbonate and supplied to the IC system at an isocratic flow of 1.2 mL/min. A sample IC spectrum is shown in Fig. 13.

NO and NO_2 Quantification

An FTIR (Jasco – 6700) equipped with a gas flow cell was utilized to analyze the gas phase effluent. Calibration curves for NO and NO_2 were generated by flowing dilutions of 1000 ppm gas standards generated with a mass flow controller (Brooks, 5850E) and balanced with N_2 at the same total flow rate as the experimental conditions (3.4 L/min). For NO the band at 1917.86 cm^{-1} was used for quantification while for NO_2 the band at 1637.78 cm^{-1} was utilized. The following instrument conditions were used for all FTIR measurements: 8 accumulations, 0.25 cm^{-1} resolution, 32 gain, 1.8 mm aperture, and

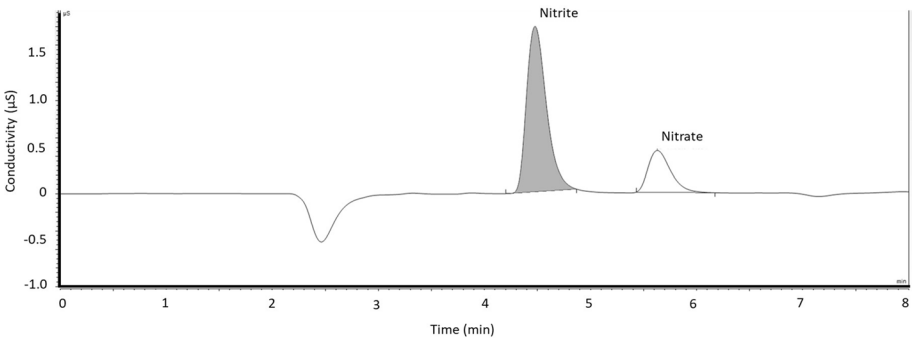

Fig. 13 Sample IC spectrum for 28% N_2 with balance argon as the carrier gas

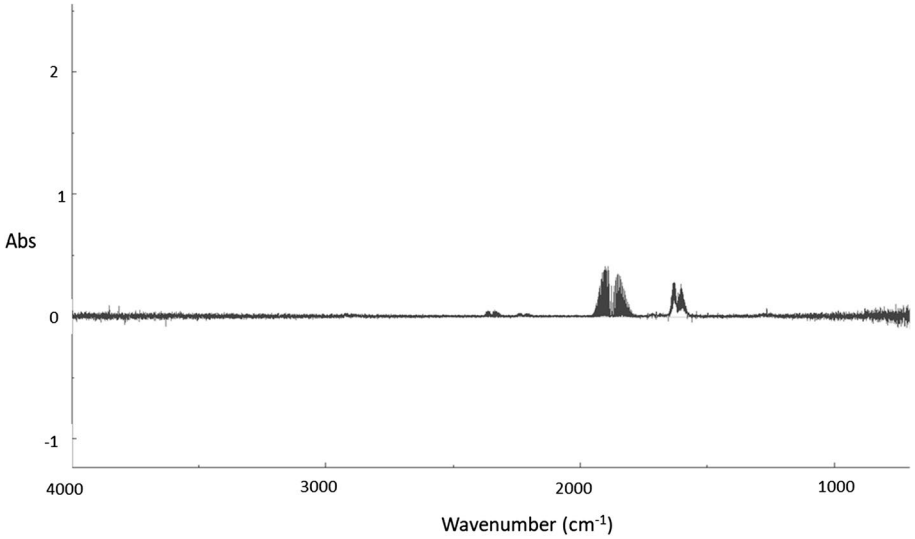

Fig. 14 Sample FTIR spectrum for 28% N_2 with balance Ar as the carrier gas

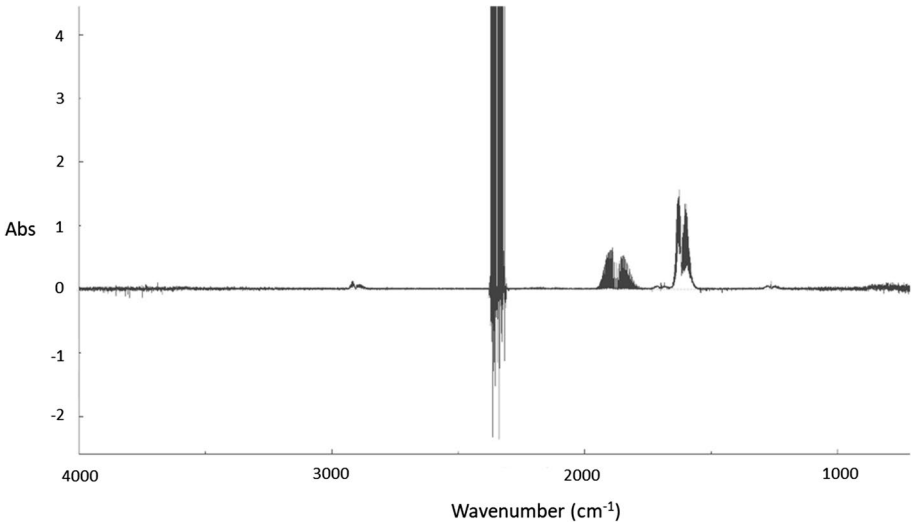

Fig. 15 Sample FTIR spectrum for air as the carrier gas

2 mm/s scanning speed. Prior to measurements the gas flow cell was purged with N_2 to remove water and air. All measurements were taken after a steady state in the flow cell had been reached by ensuring no change in the intensity of the bands for a period of two minutes. Sample experimental FTIR spectra are shown in Figs. 14 and 15.

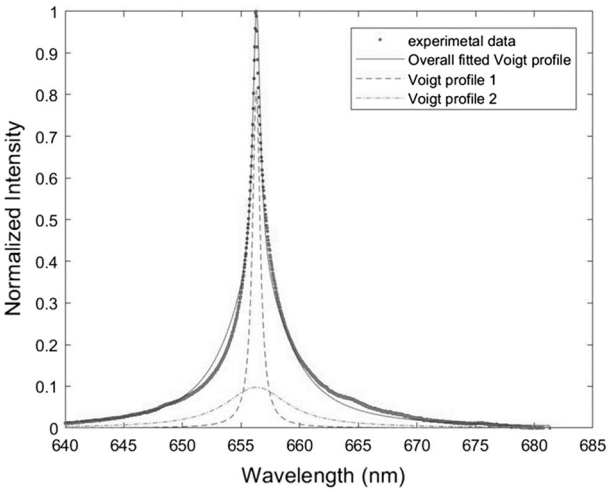

Fig. 16 H_α peak fitting in argon discharge by two Voigt profile for 28% N_2 in argon

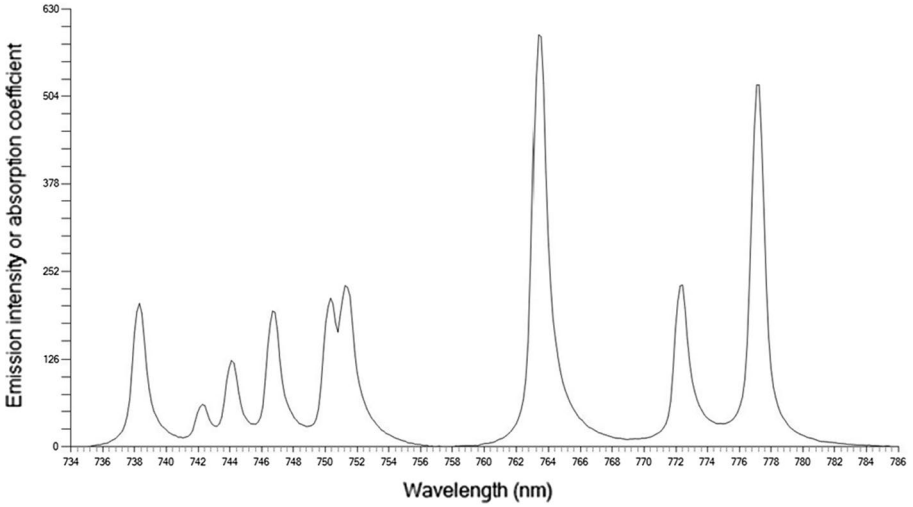

Fig. 17 Optical emission spectra for 28% nitrogen in argon showing a band at 777 nm which indicates presence of atomic oxygen

Optical Emission Spectroscopy

For OES measurements the probe tip was oriented towards the center of the discharge region in as close proximity as possible to the quartz reactor body (approx. 5 mm). Stark broadening of the H_α peak was utilized for estimation of the electron density. The H_α peak was observed using an optical emission microscope (Avantes, AvaSpec-ULS3848; wavelength range: 600–700 nm) at 656.3 nm. The H_α peak was deconvoluted into two Voigt profile. The Voigt profile was then deconvoluted into Gaussian and Lorentz profiles. The FWHM of Gaussian profile was determined by Doppler and instrument broadening where Doppler broadening was obtained using gas temperature, and instrumental broadening was obtained by calculating the FWHM of the spectral line with the

optical fiber connected to a mercury-argon lamp (Avalight-CAL). The FWHM of the Stark broadening was calculated from the relationship between the FWHM of the Van der Waal's broadening and the FWHM of the Lorentzian profile. More details of this method can be found in a previous publication and a sample of the peak fitting can be found in Figs. 16 and 17 [63].

References

1. Fridman AA (2008) Plasma chemistry. Cambridge University Press, Cambridge
2. Locke BR, Lukes P, Brisset JL (2012) Elementary chemical and physical phenomena in electrical discharge plasma in gas–liquid environments and in liquids. In: Parvulescu MMVI, Lukes P (eds) Plasma chemistry and catalysis in gases and liquids. Wiley-VCH Verlag GmbH & Co. KGaA, Weinheim
3. Lukes P, Locke BR, Brisset JL (2012) Aqueous-phase chemistry of electrical discharge plasma in water and in gas-liquid environments. In: Parvulescu MMVI, Lukes P (eds) Plasma chemistry and catalysis in gases and liquids. Wiley-VCH Verlag GmbH & Co. KGaA, Weinheim
4. Patil B, Wang Q, Hessel V, Lang J (2015) Plasma N_2-fixation: 1900–2014. Catal Today 256:49–66
5. Itikawa Y (2009) Cross sections for electron collisions with oxygen molecules. J Phys Chem Ref Data 38(1):1–20
6. Polak LS, Slovetsky DI, Todesaite RD (1975) Sov Phys High Energy Chem 9:142
7. Azizov RI, Zhivotov VK, Krotov MF, Rusanov VD, Tarasov YV, Fridman AA, Sholin GV (1980) Synthesis of nitrogen oxides in a nonequilibrium UHF discharge under electron cyclotron resonance conditions. Sov Phys High Energy Chem 14(4):275–277
8. Mizuno A, Shimizu K, Chakrabarti A, Dascalescu L, Furuta S (1995) NO_x removal process using pulsed discharge plasma. IEEE Trans Ind Appl 31(5):957–963
9. van Veldhuizen EM, Rutgers WR, Bityurin VA (1996) Energy efficiency of NO removal by pulsed corona discharges. Plasma Chem Plasma Proc 16(2):227–247
10. Yamamoto T, Yang CL, Beltran MR, Kravets Z (2000) Plasma-assisted chemical process for NOx control. IEEE Trans Ind Appl 36(3):923–927
11. Wang ZH, Li B, Ehn A, Sun ZW, Li ZS, Bood J, Alden M, Cen KF (2010) Investigation of fluegas treatment with O_3 injection using NO and NO_2 planar laser-induced fluorescence. Fuel 89(9):2346–2352
12. Huang LW, Matsuda H (2004) Removal of NO by a pulsed-corona reactor combined with in situ absorption. AIChE J 50(11):2676–2681
13. Lin H, Gao X, Luo ZY, Cen KF, Pei MX, Huang Z (2004) Removal of NO_x from wet flue gas by corona discharge. Fuel 83(9):1251–1255
14. Mok YS (2006) Absorption-reduction technique assisted by ozone injection and sodium sulfide for NO_x removal from exhaust gas. Chem Eng J 118(1–2):63–67
15. Wang ZH, Zhou JH, Fan JR, Cen KF (2006) Direct numerical simulation of ozone injection technology for NO_x control in flue gas. Energy Fuels 20(6):2432–2438
16. Mok YS, Kim JH, Nam IS, Ham SW (2000) Removal of NO and formation of byproducts in a positive-pulsed corona discharge reactor. Ind Eng Chem Res 39(10):3938–3944
17. Hu XD, Zhao GB, Legowski SF, Radosz M (2005) Moisture effect on NO_x conversion in a nonthermal plasma reactor. Environ Eng Sci 22(6):854–869
18. Yin SE, Sun BM, Gao XD, Xiao HP (2009) The effect of oxygen and water vapor on nitric oxide conversion with a dielectric barrier discharge reactor. Plasma Chem Plasma Process 29(6):421–431
19. Morgan MM, Cuddy MF, Fisher ER (2010) Gas-phase chemistry in inductively coupled plasmas for NO removal from mixed gas systems. J Phys Chem A 114(4):1722–1733
20. Yan K, Kanazawa S, Ohkubo T, Nomoto Y (1999) Oxidation and reduction processes during NO_x removal with corona-induced nonthermal plasma. Plasma Chem Plasma Process 19(3):421–443
21. Li D, Xiao Z, Aftab TB, Xu S (2018) Flue gas denitration by wet oxidation absorption methods: current status and development. Environ Eng Sci 35(11):1151–1164
22. Jogi I, Erme K, Levoll E, Raud J, Stamate E (2018) Plasma and catalyst for the oxidation of NO_x. Plasma Sources Sci Technol 27(3):035001
23. Talebizadeh P, Babaie M, Brown R, Rahimzadeh H, Ristovski Z, Arai M (2014) The role of nonthermal plasma technique in NOx treatment: a review. Renew Sustain Energy Rev 40:886–901

24. Kim HH (2004) Nonthermal plasma processing for air-pollution control: a historical review, current issues, and future prospects. Plasma Process Polym 1(2):91–110
25. Beckers F, Hoeben W, Pemen AJM, van Heesch EJM (2013) Low-level NO_x removal in ambient air by pulsed corona technology. J Phys D Appl Phys 46(29):6
26. Zhao GB, Garikipati SVB, Hu XD, Argyle MD, Radosz M (2005) Effect of oxygen on nonthermal plasma reactions of nitrogen oxides in nitrogen. AIChE J 51(6):1800–1812
27. Sathiamoorthy G, Kalyana S, Finney WC, Clark RJ, Locke BR (1999) Chemical reaction kinetics and reactor modeling of NO_x removal in a pulsed streamer corona discharge reactor. Ind Eng Chem Res 38:1844–1855
28. Huiskamp T, Hoeben W, Beckers F, van Heesch EJM, Pemen AJM (2017) (Sub)nanosecond transient plasma for atmospheric plasma processing experiments: application to ozone generation and NO removal. J Phys D Appl Phys 50(40):16
29. Chirumamilla VR, Hoeben W, Beckers F, Huiskamp T, Van Heesch EJM, Pemen AJM (2016) Experimental investigation on the effect of a microsecond pulse and a nanosecond pulse on NO removal using a pulsed DBD with catalytic materials. Plasma Chem Plasma Process 36(2):487–510
30. Matsumoto T, Wang DY, Namihira T, Akiyama H (2010) Energy efficiency improvement of nitric oxide treatment using nanosecond pulsed discharge. IEEE Trans Plasma Sci 38(10):2639–2643
31. Matsumoto T, Wang D, Namihira T, Akiyama H (2011) Process performances of 2 ns pulsed discharge plasma. Jpn J Appl Phys. https://doi.org/10.1143/JJAP.50.08JF14
32. Itikawa Y, Mason N (2005) Cross sections for electron collisions with water molecules. J Phys Chem Ref Data 34(1):1–22
33. Brisset JL, Doubla A, Amouroux J, Goldman M, Goldman A (1989) Acid-base character of species created in a point-to-plane corona discharge. 1. Acid effect of the active changeless species. Revue Internationale Des Hautes Temperatures Et Des Refractaires 25(4):229–236
34. Brisset JL, Lelievre J, Doubla A, Amouroux J (1990) Interactions with aqueous solutions of the air corona products. Revue de Physique Appliquee 25:535–543
35. Lelievre J, Dubreuil N, Brisset JL (1995) Electrolysis processes in D.C. corona discharges in humid air. J Phys III France 5:447–457
36. Benstaali B, Boubert P, Cheron BG, Addou A, Brisset JL (2002) Density and rotational temperature measurements of the OH and NO radicals produced by a gliding arc in humid air. Plasma Chem Plasma Process 22(4):553–571
37. Brisset JL, Hnatiuc E (2012) Peroxynitrite: a re-examination of the chemical properties of non-thermal discharges burning in air over aqueous solutions. Plasma Chem Plasma Process 32(4):655–674
38. Daito S, Tochikubo F, Watanabe T (2000) Improvement of NO_x removal efficiency assisted by aqueous-phase reaction in corona discharge. Jpn J Appl Phys Pt 1 39(8):4914–4919
39. Xie DY, Sun Y, Zhu TL, Ding L (2016) Removal of NO in mist by the combination of plasma oxidation and chemical absorption. Energy Fuels 30(6):5071–5076
40. Takehana K, Kuroki T, Okubo M (2018) Evaluation on nitrogen oxides and nanoparticle removal and nitrogen monoxide generation using a wet-type nonthermal plasma reactor. J Phys D Appl Phys 51(20):11
41. Burlica R, Locke BR (2008) Pulsed plasma gliding arc discharges with water spray. IEEE Trans Ind Appl 44(2):482–489
42. Burlica R, Shih KY, Locke BR (2010) Formation of H_2 and H_2O_2 in a water-spray gliding arc nonthermal plasma reactor. Ind Eng Chem Res 49(14):6342–6349
43. Wandell R, Locke B (2014) Low power pulsed plasma discharge in a water film reactor. IEEE Trans Plasma Sci in press
44. Burlica R, Kirkpatrick M, Locke B (2006) Formation of reactive species in gliding arc discharges with liquid water. J Electrostat 64(1):35–43
45. Seinfeld JH, Pandis SN (1998) Atmospheric chemistry and physics. Wiley, New York
46. Malik MA (2016) Nitric oxide production by high voltage electrical discharges for medical uses: a review. Plasma Chem Plasma Process 36(3):737–766
47. Patil BS, Peeters FJJ, van Rooij GJ, Medrano JA, Gallucci F, Lang J, Wang Q, Hessel V (2018) Plasma assisted nitrogen oxide production from air: using pulsed powered gliding arc reactor for a containerized plant. AIChE J 64(2):526–537
48. Thirumdas R, Kothakota A, Annapure U, Siliveru K, Blundell R, Gatt R, Valdramidis VP (2018) Plasma activated water (PAW): chemistry, physico-chemical properties, applications in food and agriculture. Trends Food Sci Technol 77:21–31
49. Jablonowski H, von Woedtke T (2015) Research on plasma medicine-relevant plasma-liquid interaction: What happened in the past five years? Clin Plasma Med 3(2):42–52

50. Cherkasov N, Ibhadon AO, Fitzpatrick P (2015) A review of the existing and alternative methods for greener nitrogen fixation. Chem Eng Process 90:24–33
51. He Y, Chen ZW, Li Z, Niu GD, Tang J (2018) Non-thermal plasma fixing of nitrogen into nitrate: solution for renewable electricity storage? Front Optoelectron 11(1):92–96
52. Wang WZ, Patil B, Heijkers S, Hessel V, Bogaerts A (2017) Nitrogen fixation by gliding arc plasma: better insight by chemical kinetics modelling. Chemsuschem 10(10):2145–2157
53. Liu ZC, Liu DX, Chen C, Li D, Yang AJ, Rong MZ, Chen HL, Kong MG (2015) Physicochemical processes in the indirect interaction between surface air plasma and deionized water. J Phys D Appl Phys 48(49):20
54. Liu DX, Liu ZC, Chen C, Yang AJ, Li D, Rong MZ, Chen HL, Kong MG (2016) Aqueous reactive species induced by a surface air discharge: heterogeneous mass transfer and liquid chemistry pathways. Sci Rep. https://doi.org/10.1038/srep23737
55. Liu ZC, Liu DX, Chen C, Liu ZJ, Yang AJ, Rong MZ, Chen HL, Kong MG (2018) Post-discharge evolution of reactive species in the water activated by a surface air plasma: a modeling study. J Phys D Appl Phys 51(17):12
56. Brisset JL, Moussa D, Doubla A, Hnatiuc E, Hnatiuc B, Youbi GK, Herry JM, Naitali M, Bellon-Fontaine MN (2008) Chemical reactivity of discharges and temporal post-discharges in plasma treatment of aqueous media: examples of gliding discharge treated solutions. Ind Eng Chem Res 47(16):5761–5781
57. Brisset JL, Pawlat J (2016) Chemical effects of air plasma species on aqueous solutes in direct and delayed exposure modes: discharge, post-discharge and plasma activated water. Plasma Chem Plasma Process 36(2):355–381
58. Lukes P, Dolezalova E, Sisrova I, Clupek M (2014) Aqueous-phase chemistry and bactericidal effects from an air discharge plasma in contact with water: evidence for the formation of peroxynitrite through a pseudo-second-order post-discharge reaction of H_2O_2 and HNO_2. Plasma Sources Sci Technol 23(1):15
59. Su ZZ, Ito K, Takashima K, Katsura S, Onda K, Mizuno A (2002) OH radical generation by atmospheric pressure pulsed discharge plasma and its quantitative analysis by monitoring CO oxidation. J Phys D Appl Phys 35:3192–3198
60. Wandell RJ, Wang HH, Tachibana K, Makled B, Locke BR (2018) Nanosecond pulsed plasma discharge over a flowing water film: characterization of hydrodynamics, electrical, and plasma properties and their effect on hydrogen peroxide generation. Plasma Process Polym. https://doi.org/10.1002/ppap.201800008
61. Eisenberg GM (1943) Colorimetric determination of hydrogen peroxide. Ind Eng Chem Anal Ed 15(5):327–328
62. Wang HH, Wandell RJ, Locke BR (2018) The influence of carrier gas on plasma properties and hydrogen peroxide production in a nanosecond pulsed plasma discharge generated in a water-film plasma reactor. J Phys D Appl Phys 51(9):13
63. Wang H, Wandell R, Tachibana K, Vorac J, Locke B (2018) The Influence of liquid conductivity on electrical breakdown and hydrogen peroxide production in a nanosecond pulsed plasma discharge generated in a water-film plasma reactor. J Phys D Appl Phys. https://doi.org/10.1088/1361-6463/aaf132
64. Vorac J, Synek P, Potocnakova L, Hnilica J, Kudrle V (2017) Batch processing of overlapping molecular spectra as a tool for spatio-temporal diagnostics of power modulated microwave plasma jet. Plasma Sources Sci Technol 26(2):12
65. Voráč J, Synek P, Procházka V, Hoder T (2017) State-by-state emission spectra fitting for non-equilibrium plasmas: OH spectra of surface barrier discharge at argon/water interface. arXiv preprint arXiv:1703.09978
66. Nikiforov AY, Leys C, Gonzalez MA, Walsh JL (2015) Electron density measurement in atmospheric pressure plasma jets: stark broadening of hydrogenated and non-hydrogenated lines. Plasma Sources Sci Technol 24(3):18
67. Zhu XM, Walsh JL, Chen WC, Pu YK (2012) Measurement of the temporal evolution of electron density in a nanosecond pulsed argon microplasma: using both Stark broadening and an OES line-ratio method. J Phys D Appl Phys 45(29):11
68. Lieberman M, Lichtenberg A (2005) Principles of plasma discharge and materials processing, 2nd edn. John Wiley & Sons, Hoboken
69. Hagelaar GJM, Pitchford LC (2005) Solving the Boltzmann equation to obtain electron transport coefficients and rate coefficients for fluid models. Plasma Sources Sci Technol 14(4):722–733
70. Janda M, Martišovitš V, Hensel K, Machala Z (2016) Study of transient spark discharge focused at NO*x* generation for biomedical applications. J Phys Conf Ser 768(1):012009

71. Janda M, Martisovits V, Hensel K, Machala Z (2016) Generation of antimicrobial NO*x* by atmospheric air transient spark discharge. Plasma Chem Plasma Process 36(3):767–781
72. Janda M, Hensel K, Machala Z (2018) Kinetic plasma chemistry model of pulsed transient spark discharge in air coupled with nanosecond time-resolved imaging and spectroscopy. J Phys D Appl Phys 51(33):10
73. Tarabova B, Lukes P, Janda M, Hensel K, Sikurova L, Machala Z (2018) Specificity of detection methods of nitrites and ozone in aqueous solutions activated by air plasma. Plasma Process Polym 15(6):12
74. Locke BR, Shih KY (2011) Review of the methods to form hydrogen peroxide in electrical discharge plasma with liquid water. Plasma Sources Sci Technol 20(3):15
75. Locke BR, Thagard SM (2012) Analysis and review of chemical reactions and transport processes in pulsed electrical discharge plasma formed directly in liquid water. Plasma Chem Plasma Process 32(5):875–917
76. Mededovic S, Locke BR (2007) Primary chemical reactions in pulsed electrical discharge channels in water. J Phys D Appl Phys 40(24):7734–7746
77. Hofmann S, van Gessel AFH, Verreycken T, Bruggeman P (2011) Power dissipation, gas temperatures and electron densities of cold atmospheric pressure helium and argon RF plasma jets. Plasma Sources Sci Technol 20(6):12
78. Hsieh KC, Wandell RJ, Bresch S, Locke BR (2017) Analysis of hydroxyl radical formation in a gas-liquid electrical discharge plasma reactor utilizing liquid and gaseous radical scavengers. Plasma Process Polym 14(8):14
79. Lindsay A, Byrns B, King W, Andhvarapou A, Fields J, Knappe D, Fonteno W, Shannon S (2014) Fertilization of radishes, tomatoes, and marigolds using a large-volume atmospheric glow discharge. Plasma Chem Plasma Process 34(6):1271–1290
80. Bian WJ, Song XH, Shi JW, Yin XL (2012) Nitrogen fixed into HNO_3 by pulsed high voltage discharge. J Electrostat 70(3):317–326
81. Hessel V, Anastasopoulou A, Wang Q, Kolb G, Lang J (2013) Energy, catalyst and reactor considerations for (near)-industrial plasma processing and learning for nitrogen-fixation reactions. Catal Today 211:9–28
82. van Ham BTJ, Hofmann S, Brandenburg R, Bruggeman PJ (2014) In situ absolute air, O_3 and NO densities in the effluent of a cold RF argon atmospheric pressure plasma jet obtained by molecular beam mass spectrometry. J Phys D Appl Phys 47(22):9
83. Park DP, Davis K, Gilani S, Alonzo CA, Dobrynin D, Friedman G, Fridman A, Rabinovich A, Fridman G (2013) Reactive nitrogen species produced in water by non-equilibrium plasma increase plant growth rate and nutritional yield. Curr Appl Phys 13:S19–S29
84. Su ZZ, Ito K, Takashima K, Katsura S, Onda K, Mizuno A (2002) OH radical generation by atmospheric pressure pulsed discharge plasma and its quantitative analysis by monitoring CO oxidation. J Phys D Appl Phys 35(24):3192–3198
85. Tang XL, Wang JG, Yi HH, Zhao SZ, Gao FY, Chu C (2018) Nitrogen fixation and NO conversion using dielectric barrier discharge reactor: identification and evolution of products. Plasma Chem Plasma Process 38(3):485–501
86. Pavlovich MJ, Ono T, Galleher C, Curtis B, Clark DS, Machala Z, Graves DB (2014) Air spark-like plasma source for antimicrobial NO*x* generation. J Phys D Appl Phys 47(50):10
87. Wandell RJ, Bresch S, Hsieh K, Alabugin IV, Locke BR (2014) Formation of alcohols and carbonyl compounds from hexane and cyclohexane with water in a liquid film plasma reactor. IEEE Trans Plasma Sci 42(5):1195–1205